



Line-of-Sight Velocity As a Tracer of Coronal Cavity Magnetic Structure

Urszula Bąk-Stęślička^{1*}, Sarah E. Gibson² and Ewa Chmielewska¹

¹ Astronomical Institute, University of Wrocław, Wrocław, Poland, ² High Altitude Observatory, National Center for Atmospheric Research, Boulder, CO, USA

We present a statistical analysis of 66 days of observations of quiescent (non-erupting) coronal cavities and associated velocity and thermal structures. We find that nested rings of LOS-oriented velocity are common in occurrence and spatially well correlated with cavities observed in emission. We find that the majority of cavities possess multiple rings, and a range in velocity on the order of several *km/sec*. We find that the tops of prominences lie systematically below the cavity center and location of largest Doppler velocity. Finally, we use DEM analysis to consider the temperature structure of two cavities in relation to cavity, prominence, and flows. These observations yield new constraints on the magnetic structure of cavities, and on the conditions leading up to solar eruptions.

Keywords: sun: corona, sun: filaments, prominence, sun: infrared, sun: magnetic field

OPEN ACCESS

Edited by:

Xueshang Feng,
National Space Science Center, China

Reviewed by:

Gordon James Duncan Petrie,
National Solar Observatory, USA
Chaowei Jiang,
Chinese Academy of Sciences, China

*Correspondence:

Urszula Bąk-Stęślička
bak@astro.uni.wroc.pl

Specialty section:

This article was submitted to
Stellar and Solar Physics,
a section of the journal
Frontiers in Astronomy and Space
Sciences

Received: 08 January 2016

Accepted: 19 February 2016

Published: 18 March 2016

Citation:

Bąk-Stęślička U, Gibson SE and
Chmielewska E (2016) Line-of-Sight
Velocity As a Tracer of Coronal Cavity
Magnetic Structure.
Front. Astron. Space Sci. 3:7.
doi: 10.3389/fspas.2016.00007

1. INTRODUCTION

Solar coronal cavities are regions of rarefied density and elliptical cross-section (Fuller and Gibson, 2009; Gibson et al., 2010; Forland et al., 2013). They are often observed in eruption as a component of the classic three-part structure of a Coronal Mass Ejections (CME), as they surround the CME's bright core formed by the dense material from the eruptive prominence (Illing and Hundhausen, 1986; Tandberg-Hanssen, 1995). Cavities exist not only as eruptive phenomena, however. Non-erupting, or quiescent cavities may exist in equilibrium for many days or weeks (Gibson et al., 2006). They usually surround quiescent prominences (Tandberg-Hanssen, 1995), especially in the polar crown regions, but in some cases cavities are observed in the absence of prominences. Cavities are mostly observed when a filament or filament channel is large and oriented along the line-of-sight, and where there are no bright neighboring structures (Gibson, 2015; McCauley et al., 2015).

The first recorded observations of cavities were made in white light (WL) during the solar eclipse of January 22, 1898 (Wesley, 1927) and since then cavities have been studied many times (Waldmeier, 1941; von Klüber, 1961; Williamson et al., 1961; Waldmeier, 1970; Gibson et al., 2006). The first explanation of the cavity phenomena as an area of reduced electron density was proposed by Waldmeier (1941). Cavities have been observed in a wide wavelength range, not only in WL, but also in radio, EUV and SXR (Vaiana et al., 1973a,b; Hudson et al., 1999; Hudson and Schwenn, 2000; Marqué et al., 2002; Marqué, 2004; Heinzel et al., 2008; Berger et al., 2012; Reeves et al., 2012). Observations in WL are particularly useful for larger cavities; smaller cavities are better viewed in EUV (Gibson, 2015). *Yohkoh*/Soft X-ray Telescope observations revealed hot central cores within cavities (Hudson et al., 1999; Hudson and Schwenn, 2000). Other analyses also suggest the existence of hotter plasma inside cavities (Fuller et al., 2008; Habbal et al., 2010; Reeves et al., 2012).

Cavities have been modeled as a flux rope (Low, 1994; Low and Hundhausen, 1995), but the physical nature of cavities is still under investigation. Although quiescent cavities are long-lived and their structure evolves slowly with time, they have been observed to bodily erupt as a CME

(Maričić et al., 2004; Vršnak et al., 2004; Gibson et al., 2006; Régnier et al., 2011; Forland et al., 2013; Su et al., 2015). Understanding the magnetic structure of such cavities may be essential for establish the pre-CME configurations and for choosing between models for CME eruptive drivers.

The Coronal Multi-channel Polarimeter (CoMP) observes the full-Sun lower coronal magnetic field via spectropolarimetric measurements of the the forbidden lines of Fe XIII. These observations give us information about line intensity (polarized and unpolarized), Doppler shift, and line width. These in turn constrain coronal density, temperature, velocity, and through the polarization measurements, magnetic field. Observations of linear polarization in particular diagnose the direction of the magnetic field in the plane of sky (POS), and are well-suited for analysis of the magnetic configuration in polar-crown prominence cavities. CoMP observations have revealed that polar-crown cavities showed characteristic structures in linear polarization (**Figure 1**) which we termed “lagomorphic,” due to their resemblance to rabbit heads seen in silhouette. This characteristic structure may be explained by a magnetic flux-rope model (Bąk-Stęślicka et al., 2013). Lagomorphic structures are very common, and they may be observed in most of the cavities oriented along the line of sight (LOS). The size of the CoMP lagomorphic signature generally scales with the cavity size seen in EUV (Bąk-Stęślicka et al., 2014).

The first CoMP observations of cavities, taken while it was placed at the National Solar Observatory in 2005, revealed interesting results. Schmit et al. (2009) found, for the first time, Doppler velocities in the range of $5 - 10 \text{ km s}^{-1}$ within a coronal cavity. In our previous paper (Bąk-Stęślicka et al., 2013) we showed another example of LOS flows within cavities. What was the most interesting about these flows was that they occurred in the form of nested ring-like structures with apparently counterstreaming velocities.

In the present work we present a statistical analysis of Doppler velocities within cavities. In Section 2 we describe the data used in our study of 66 days of cavity flow observations. In Section 3 we present our results, and discuss relations between cavities, flows,

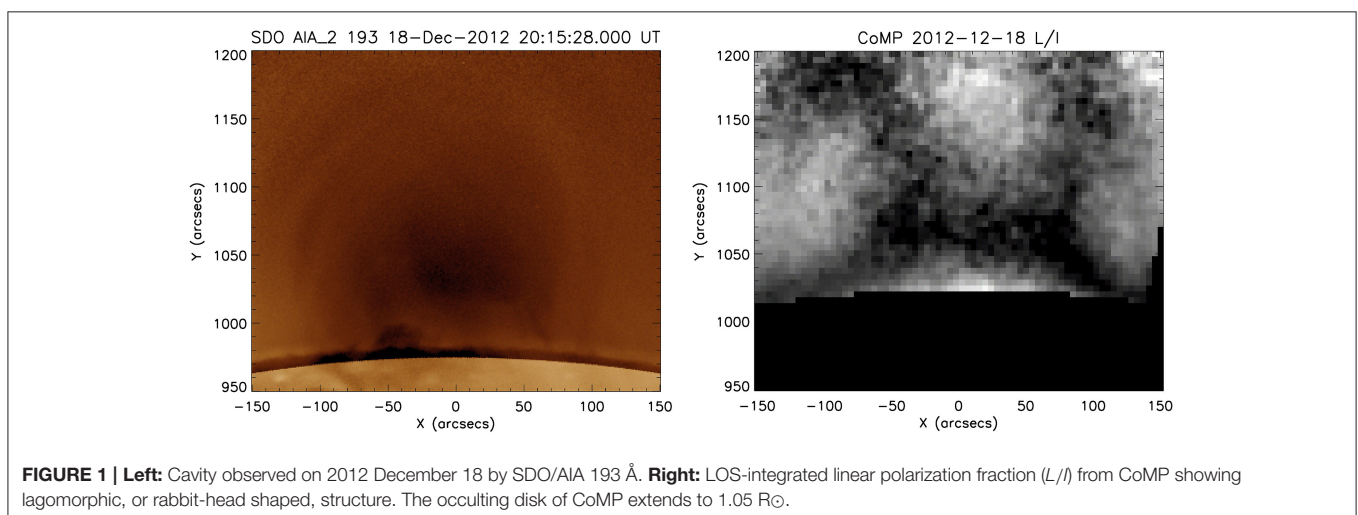
associated prominences, and hot cores. In Section 4 we give our conclusions.

2. INSTRUMENTS AND DATA ANALYSIS

2.1. Instruments

The Atmospheric Imaging Assembly (AIA, Lemen et al., 2012) on board *Solar Dynamics Observatory* (SDO, Pesnell et al., 2012) continuously makes full-disk images of the Sun through ten passbands with a spatial resolution ~ 1 arcsecond, temporal cadence of 12 s, and FOV of $1.3 R_{\odot}$. AIA consists of four telescopes and provides narrow-band imaging of seven extreme ultraviolet (EUV) band passes centered on lines: Fe XVIII (94 Å), Fe VIII, XXI (131 Å), Fe IX (171 Å), Fe XII, XXIV (193 Å), Fe XIV (211 Å), He II (304 Å), and Fe XVI (335 Å). For effective temperature diagnostics of EUV emissions these cover the range from 0.6 to 20 MK.

The CoMP was installed in 2010 at the Mauna Loa Solar Observatory (MLSO) in Hawaii. Since 2010 October CoMP has made daily (subject to weather conditions) observations of the coronal magnetic field in the lower corona with a field of view (FOV) of about 1.04–1.4 solar radii and a spatial resolution of 4.46"/pixel. CoMP measures a polarimetric signal (Stokes I, Q, U, V) of the forbidden lines of Fe XIII at 1074.7 and at 1079.8 nm (Tomczyk et al., 2008). The line-of-sight (LOS) directed strength of the magnetic field can be obtained from the circular polarization (Stokes V) although such observations require long integration times on the order of multiple hours due to the very low intensity of circular polarization. As discussed above, the direction of the magnetic field in the POS – subject to a (resolvable) 90° ambiguity – can be determined from the observations in the linear polarization. LOS velocity is obtained via Doppler line shift measurements. All measurements are integrated along the LOS since the corona is optically thin; however forward modeling and CoMP observations have demonstrated that for extended structures such as polar-crown cavities critical information is preserved (see Gibson et al., 2016).



2.2. Data Analysis

Using daily AIA 193 Å images and CoMP data we examined multiple years of polar-crown cavities and analyzed their properties. In particular, we investigated Doppler velocity patterns, quiescent prominences, and hot cores in relation to cavities.

In the set of CoMP observations between January 2012 and October 2015, we analyzed more than 70 days for which a coherent Doppler velocity pattern was observed in the cavity. For the purpose of our analysis we excluded those for which the cavity center was at a height lower than the CoMP occulter, and cavities positioned too close to the telescope occulter arm where there was no possibility of obtaining complete intensity and velocity profiles. This left us with 66 days of cavity flow observations, of which 46 appear to be independent cavity systems. We note that it is difficult to determine whether cavities are truly “independent,” since they are extended along the line of sight and may go in and out of view with a curve of the the neutral line (see Gibson et al., 2006 for further discussion). For the purposes of this paper we consider distinct days of observation as data points.

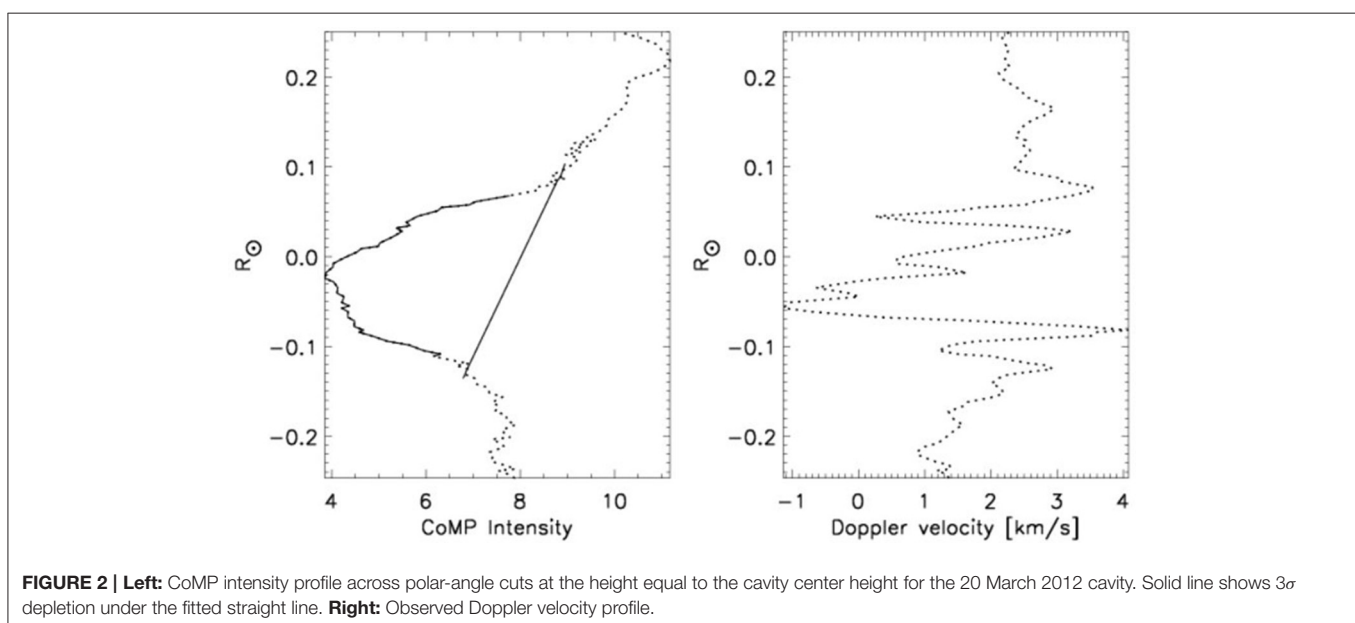
From CoMP observations we used intensity (Stokes-I) images and Doppler shift maps. We mainly used the Level 2 three-point data of the Fe XIII 1074.7 nm line taken between January 2012 and October 2015 available on the MLSO web page (<http://mlso.hao.ucar.edu>). The zero point for CoMP Doppler velocity is not currently well established (*G. de Toma., private communication*); we therefore used the median value of Doppler shift in each map as our zero point in the scale (Tian et al., 2013). In addition, both intensity and Doppler shifts images were averaged over tens of minutes to hours, to improve the signal-to-noise ratio. Such averaging may affect our obtained velocity gradient (average values are likely to be smaller than for individual moments of time). Doppler velocity for Level 2 is also partially corrected for solar rotation through a model described by Tian et al. (2013);

this model assumption may be source of uncertainty. Since cavities are relatively small compared to the velocity gradients of the Tian model, and since our analysis depends on relative velocity values rather than absolute ones, our conclusions will be generally robust to these uncertainties.

AIA 193 Å images were used to measure the height of the cavity center [a detailed description of this method can be found in Gibson et al. (2010)]. For each cavity we extracted polar-angle cuts in the averaged CoMP intensity image at the same height as the AIA cavity center height (**Figure 2**, left). Using such CoMP intensity profiles we measured an average signal at the cavity rim on both sides of the cavity, and fit a straight line between those points. We defined a cavity width using an area where the signal decreased more than 3σ in relation to the fitted line. We repeated this analysis three times. The width, presented in this paper, is the average value from those measurements and the error is their standard deviation. We note that the cavity width obtained in this manner is somewhat larger than for widths in previously reported results based on AIA data (Forland et al., 2013).

We applied the same polar-angle cuts to the Doppler velocity images and used the same averaging as for the CoMP intensity images (**Figure 2**, right). Using these cavity-center velocity profiles, we measured the velocity range (minimum to maximum) within the cavity and the position of the strongest flow. Since many cavities show a nested-rings pattern in Doppler velocity images, we also calculated the slope of the velocity profiles and number of the velocity gradient changes. We also smoothed velocity profiles (using 2, 3, and 4 points), then measured the number of the velocity gradient changes. The values presented in this paper are the averaged value (from smoothed and unsmoothed profiles), error is their standard deviation.

For two cavities we used six of the AIA filters (94, 131, 171, 193, 211, and 335 Å) to calculate Differential Emission



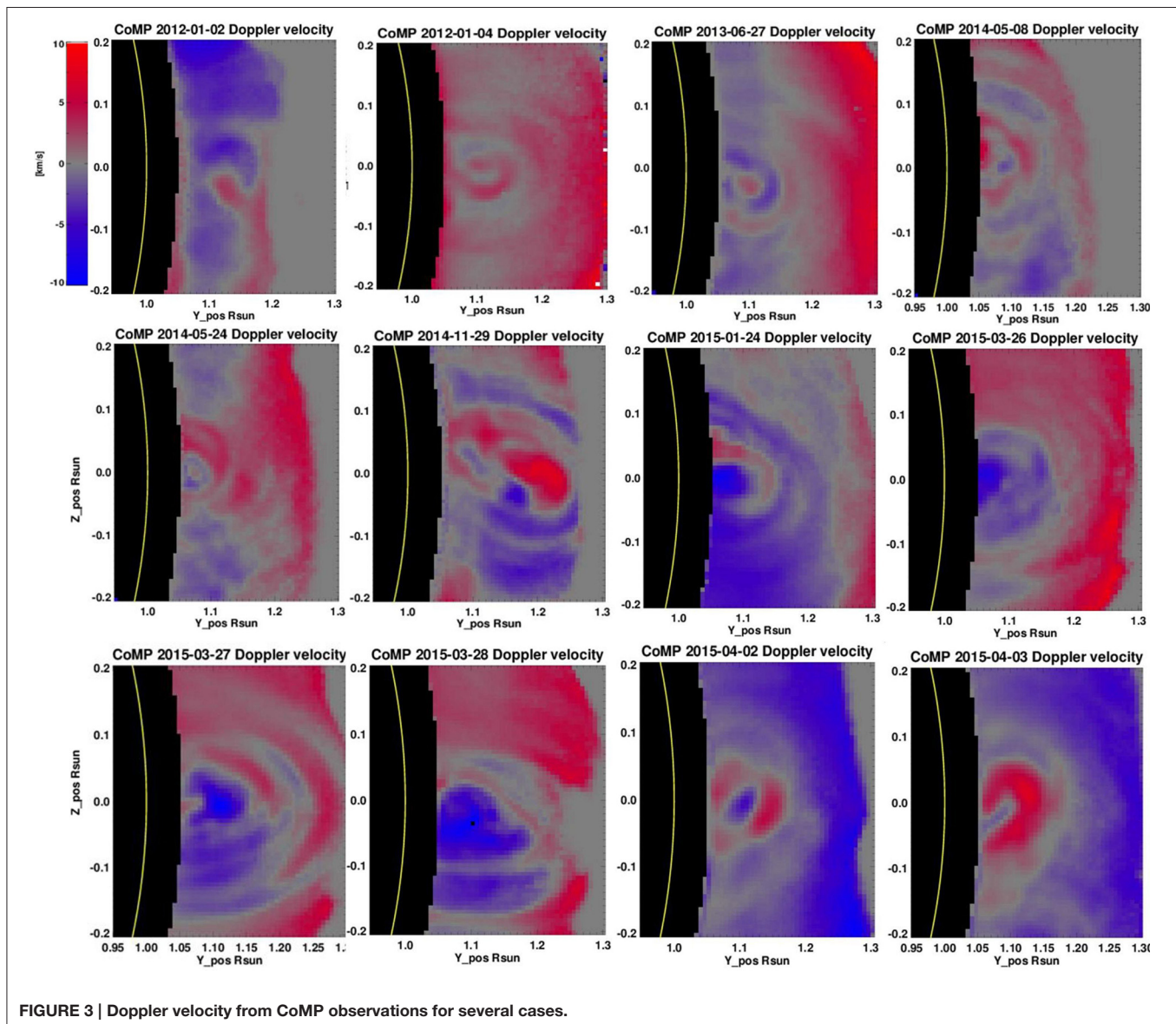
Measure (DEM). We calculated response functions for all six filters using the CHIANTI database (Dere et al., 1997). In order to calculate DEM profiles and maps we used the iterative forward-fitting method originally developed for *HINODE/XRT* data (Weber et al., 2004). This XRT method of DEM calculation is available through SSW and was slightly modified by Cheng et al. (2012) to work with the AIA filters (see Appendix of Cheng et al., 2012). In this forward fitting method the differences between fitted and the observed intensities in six EUV AIA filters are minimized. For each pixel in the map we calculated the DEM-weighted average temperature. This parameter characterizing the overall temperature was introduced by Cheng et al. (2012):

$$\bar{T} = \frac{\int DEM(T) \times T dT}{\int DEM(T) dT} \quad (1)$$

Finally, for the full set of cavities with flows, we used AIA 304 Å images to calculate the height of any associated prominence (at the top as measured in an averaged image).

3. RESULTS

First of all, we find that coherent – often ring-shaped – flows in Doppler velocity are almost as common within cavities as the “lagomorphic” signature in linear polarization discussed in our previous paper (Bąk-Stęślicka et al., 2013), although the visibility of both depends upon the orientation and extent of the cavity; see Jibben et al. (2016) for an example of a cavity which does not have a clear lagomorph/quiescent velocity structure. The flows in the 66 days we analyzed are usually in the form of the characteristic concentric rings within the cavity (**Figures 3, 4**), and may be observed to persist for a few days (as is also true for lagomorphic



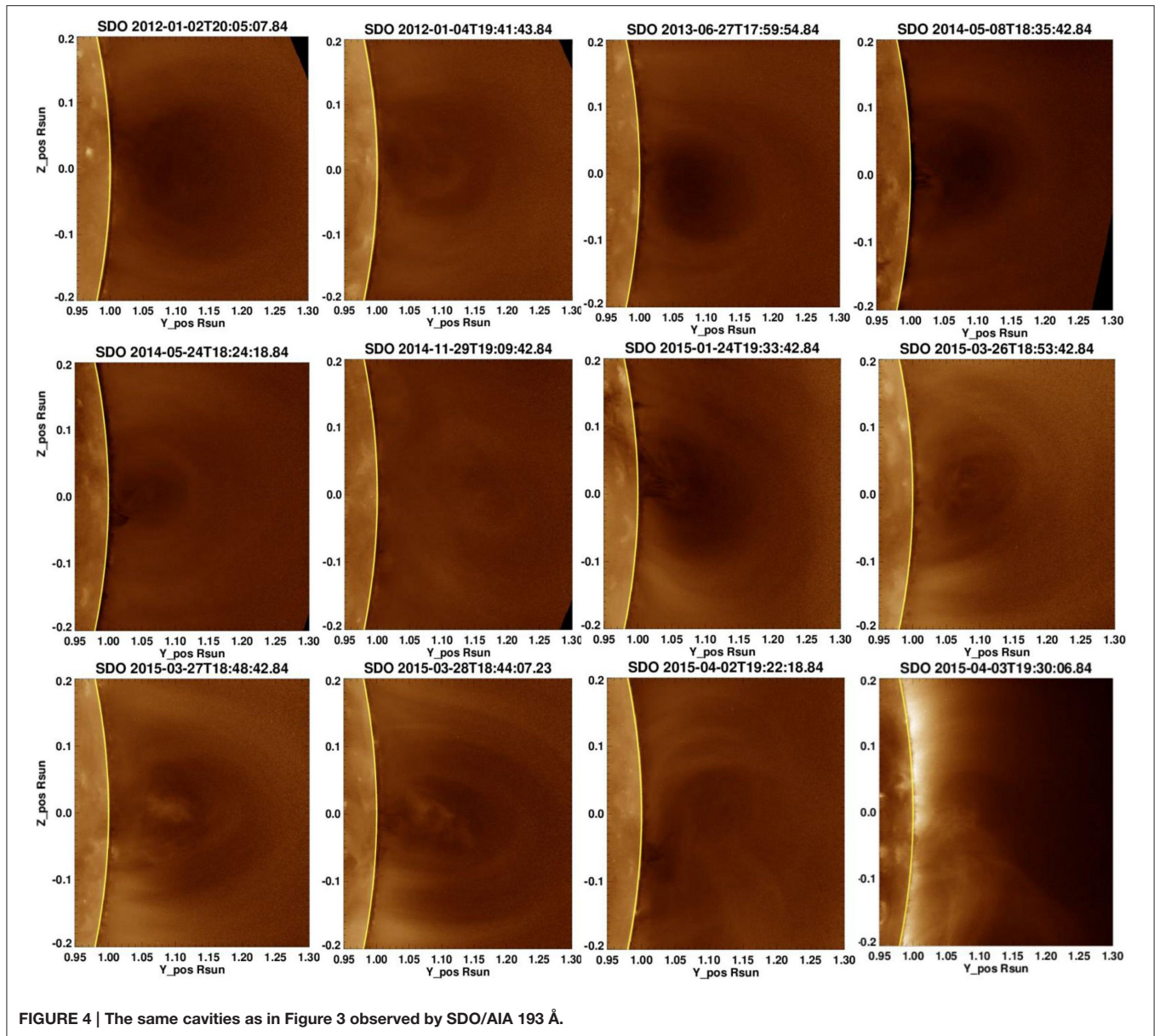


FIGURE 4 | The same cavities as in Figure 3 observed by SDO/AIA 193 Å.

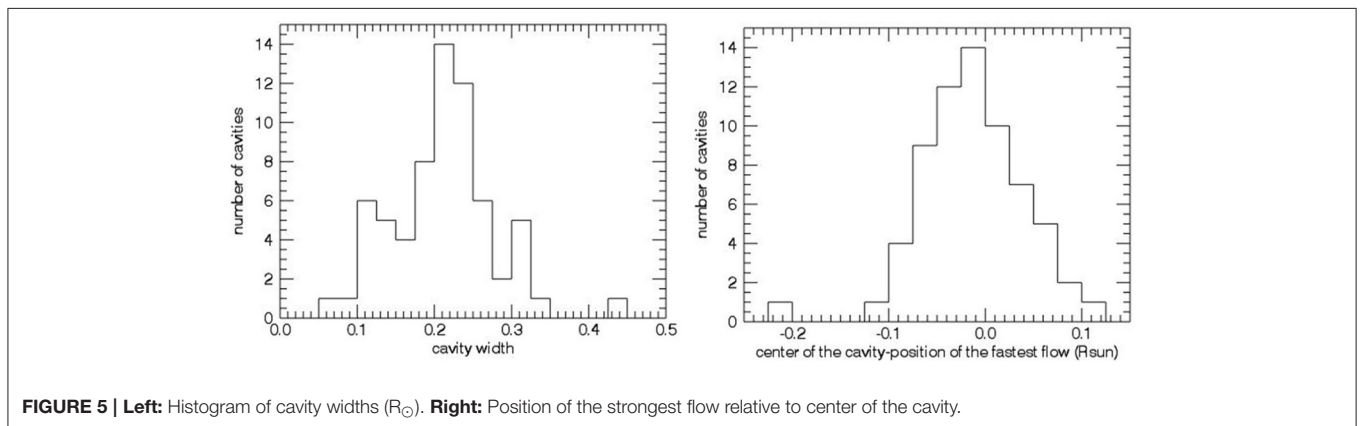


FIGURE 5 | Left: Histogram of cavity widths (R_{\odot}). Right: Position of the strongest flow relative to center of the cavity.

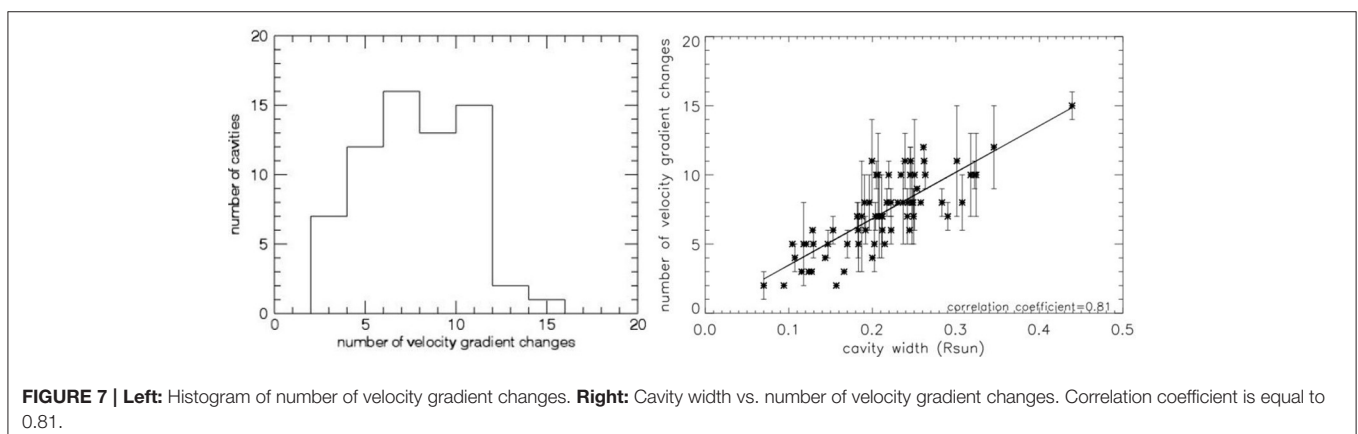
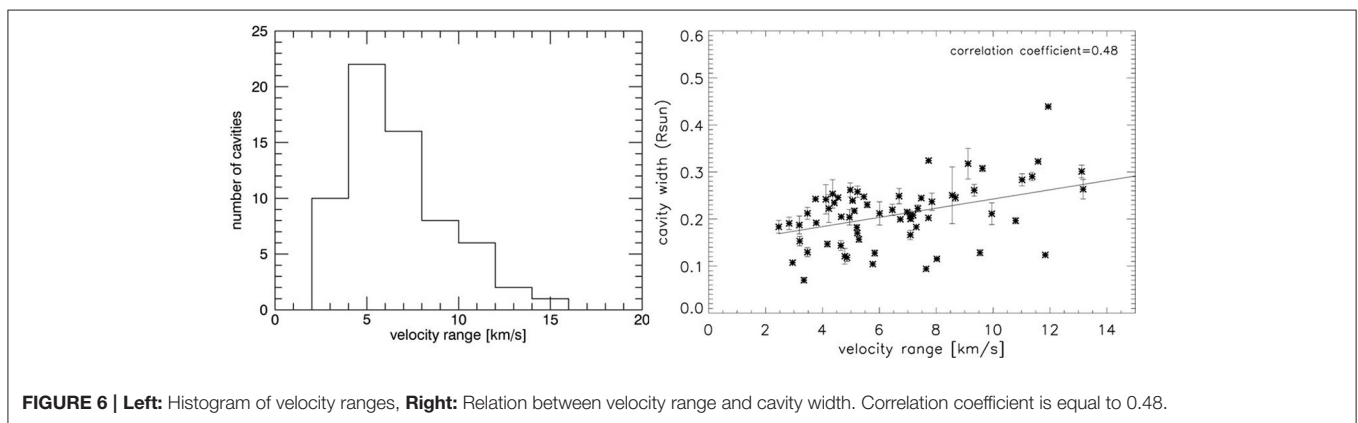
structures). Eventually, the change of the cavity's orientation as it rotates past the limb – and possibly also evolution of the structure – leads to the loss of a clearly viewed cavity, lagomorph, and velocity rings.

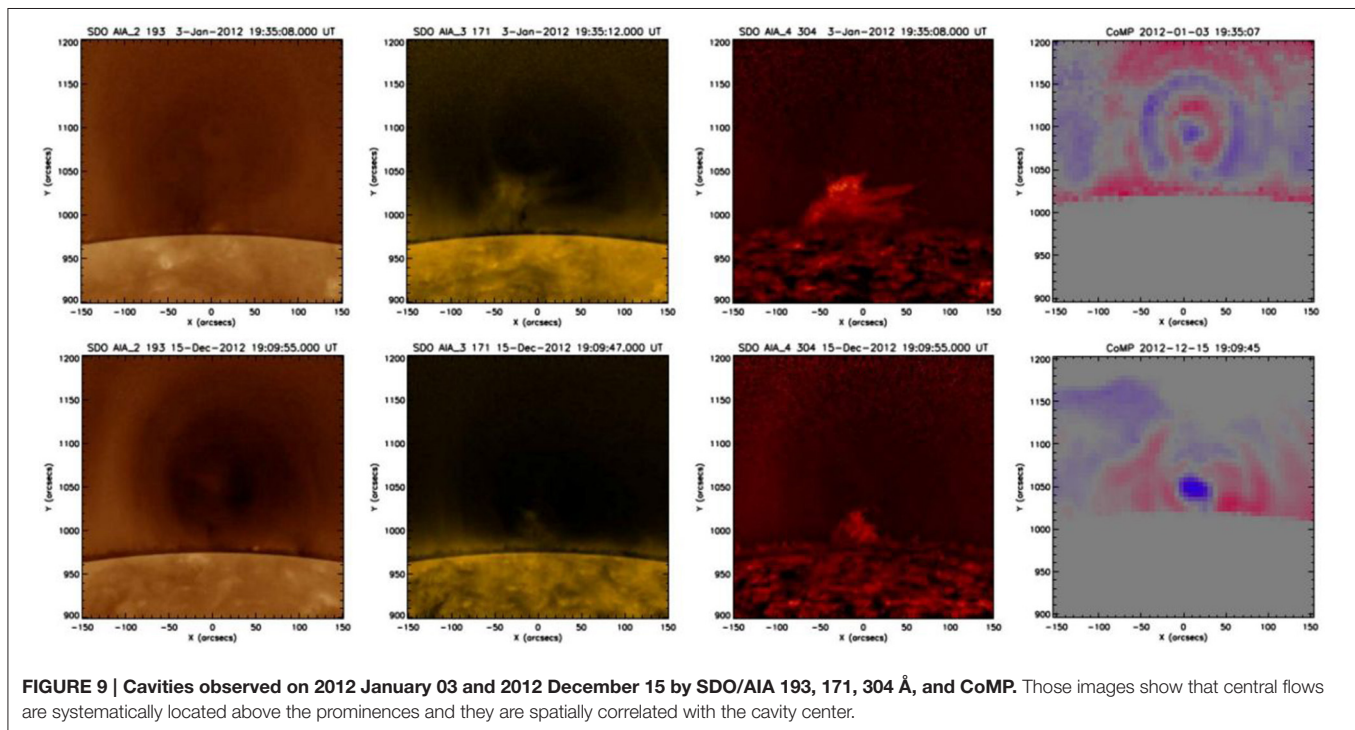
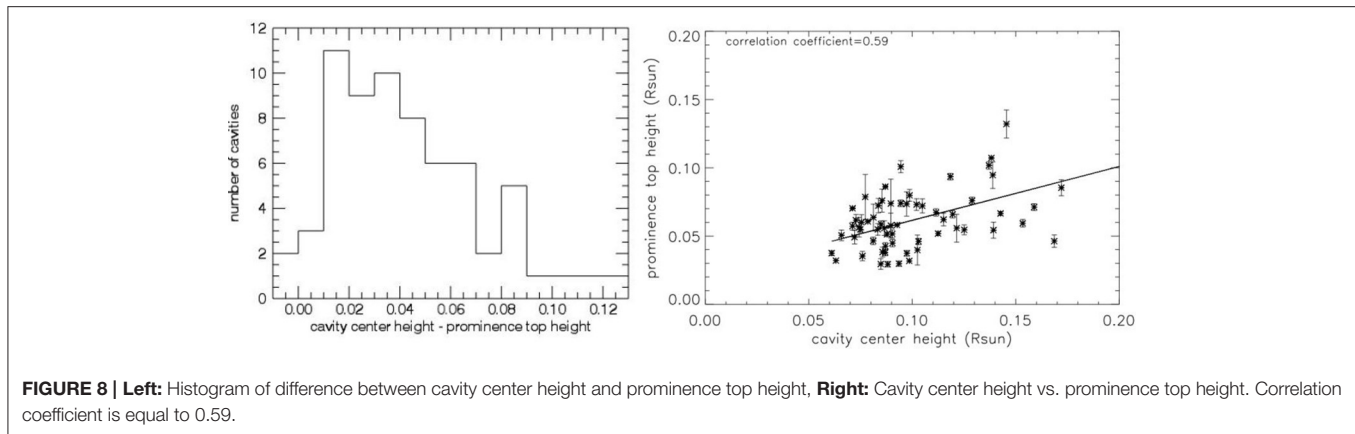
We found that almost half of the analyzed cavities have a width of about $0.2\text{--}0.25 R_{\odot}$ (**Figure 5**, left). Detailed inspection of CoMP images and the intensity and velocity profiles indicate that flows are localized within the cavity (**Figures 2–4**). A histogram comparing the position of the strongest flow to the position of the cavity center is presented in **Figure 5** (right). In most cases this difference is within $0.05 R_{\odot}$ of the cavity center which suggest that central flows are the strongest ones. In cases where the strongest flows are not observed in the center, a weaker central flow is often still present. We note that the errors in our method for finding the cavity center from AIA data are on the order $0.01 R_{\odot}$, and that there are errors in alignment between AIA and CoMP of similar or somewhat larger size. These alignment errors may have a systematic component, which could also contribute to the skew in the distribution.

In most cases the range of velocities observed within a cavity is between 4 and 8 km/s (see **Figure 6**, left), which is consistent with previous reports (Schmit et al., 2009), but larger ranges (> 10 km/s) are also sometimes observed. **Figure 6** (right) shows the relation between velocity range and cavity width. The strongest ranges in velocities are observed in the widest and largest cavities.

Because of the uncertainty in the zero point of the velocity, it is still not clear if flows are truly counterstreaming, however, velocity gradients are clearly observed. Even if concentric rings in velocity (**Figure 3**) do not imply a change in flow direction, each ring may be an indicator of a discontinuity in LOS-directed velocity. The number of loops (or whole rings for higher cavities) is thus of interest. Taking the derivative of the velocity profile we obtain the number of velocity gradient changes (if the structure were symmetric about the center, the number of loops would be half the number of gradient changes). Most cavities indicate 6 – 12 such gradient changes (see **Figure 7**, left), but this number changes with smoothing of the velocity profile (see error bars in the **Figure 7**, right). This number of changes is well correlated with the cavity width (**Figure 7**, right).

In all but three cases, we observed prominences in AIA 304 Å associated with the cavities. We analyzed the relation between cavity center height and the heights of these prominences. A histogram of the difference between the two values is presented in **Figure 8**, left. In all but two cases, the prominence top was below the cavity center and central flows (in the two cases, the prominence was only slightly higher). The prominence top heights are also correlated with the cavity height: for higher cavities, higher prominences were observed. Sample images for two cavities are presented in **Figure 9**.

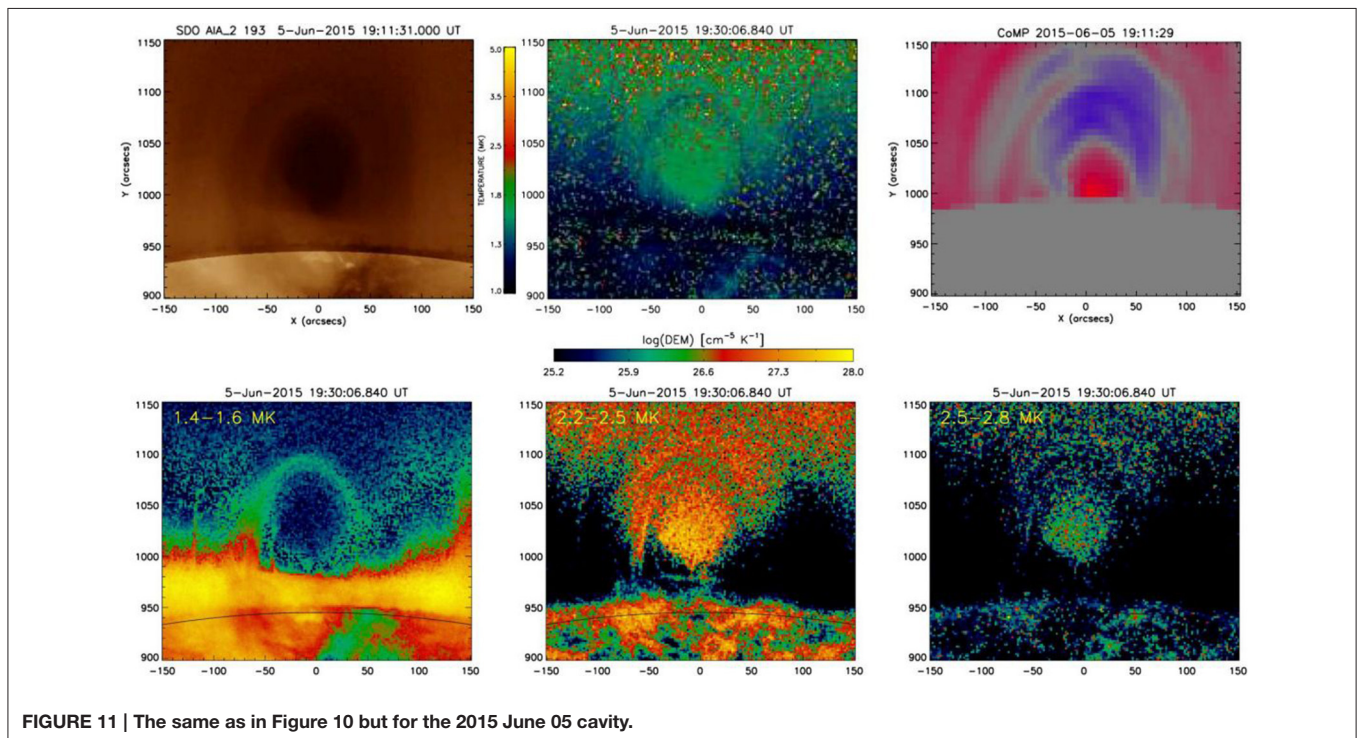
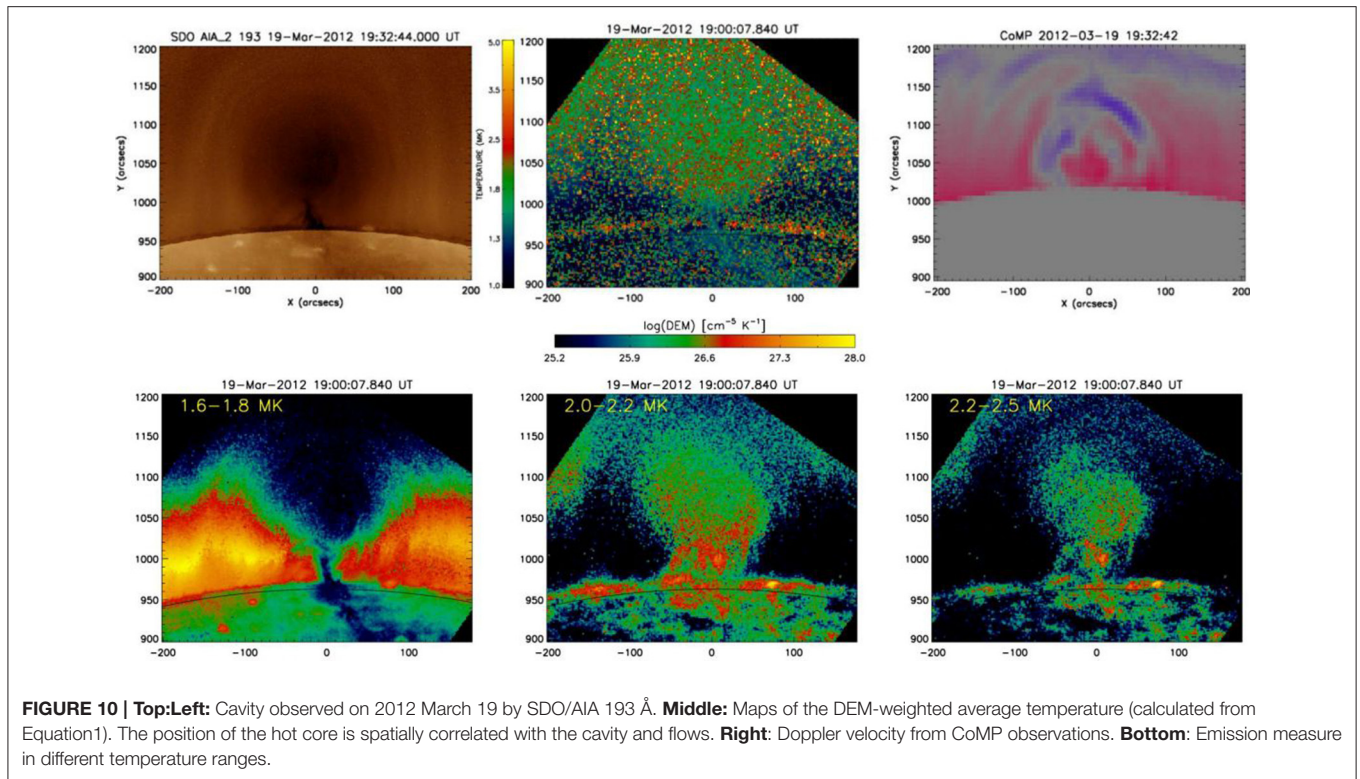




For two of the cavities we calculated DEM maps and profiles and estimated the average temperature using Equation 1. Maps characterizing the overall temperature are presented in **Figures 10, 11** (middle). In both cases, at least the central portion of the cavity seems to be filled with hotter material than its surroundings, which is consistent with results of Habbal et al. (2010). We found that the temperature in the center of these cavities were 2.3 and 2.1 MK for 2012 March 19 and 2015 June 05, respectively. The position of these hot cores is spatially correlated within the cavity seen in AIA 193 Å (**Figures 10, 11**, top panels, left) and flows (**Figures 10, 11**, top panels, right). In the second example, the position of the hot core is strongly correlated with the position of the part of the cavity with the lowest density and the strongest central flow observed by CoMP. DEM maps are presented in **Figures 10, 11** (bottom panels).

4. CONCLUSIONS

We have found that LOS-flow structure within coronal cavities is clearly related both to cavity morphology and to cool (prominence) and hot (corona) plasma distribution. Because the corona is magnetically dominated, these relations must ultimately derive from the magnetic field. The fact that prominences systematically lie below the center of cavities and the peak LOS coronal flow, indicates an association of the cavity center with a LOS-oriented, axial magnetic field. This, in combination with the concentric rings of flows surrounding this axis implies toroidal flux surfaces consistent with a magnetic flux rope topology. These observations thus provide complementary evidence toward conclusions based on previously discovered linear-polarization lagomorph signatures



within cavities. They also motivate efforts to obtain large-aperture telescope measurements of circular polarization [see further discussion in Gibson (2015)]. The details of how

these field-aligned flows originate remain uncertain, however, and represent a challenge to magnetohydrodynamic models of prominence and cavity formation.

AUTHOR CONTRIBUTIONS

UBS led the design and carried out the statistical analysis, and led the interpretation and writing of the paper. SG contributed to the design and interpretation of the analysis, and to the writing of the paper. EC did the DEM analysis. All authors read and critically revised the paper, approved the final version, and agreed to be accountable for all aspects of the work.

FUNDING

UBS and EC acknowledge financial support from the Polish National Science Centre grant 2011/03/B/ST9/00104. SG acknowledges support from the Air Force Office of Space

Research, FA9550-15-1-0030. NCAR is supported by the National Science Foundation.

ACKNOWLEDGMENTS

This work was enabled by participation of UBS and SG in the International Space Science Institute (ISSI) working group on coronal magnetism (2013–2014). AIA data were courtesy of NASA/SDO and the AIA, EVE, and HMI science teams. The CoMP data was provided courtesy of the MLSO, operated by the HAO, as part of the NCAR. We thank Giuliana de Toma and Steve Tomczyk in particular for assistance with these data, and Giuliana de Toma for internal HAO review.

REFERENCES

- Bąk-Stęślička, U., Gibson, S. E., Fan, Y., Bethge, C., Forland, B., and Rachmeler, L. A. (2013). The magnetic structure of solar prominence cavities: new observational signature revealed by coronal magnetometry. *Astrophys. J.* 770, 28. doi: 10.1088/2041-8205/770/2/L28
- Bąk-Stęślička, U., Gibson, S. E., Fan, Y., Bethge, C., Forland, B., and Rachmeler, L. A. (2014). "The spatial relation between EUV cavities and linear polarization signatures," in *Nature of Prominences and their role in Space Weather. Proceedings of the International Astronomical Union, IAU Symposium*, Vol. 300, eds B. Schmieder, J.-M. Malherbe, and S. T. Wu (Cambridge, UK: Cambridge University Press), 395–396.
- Berger, T. E., Liu, W., and Low, B. C. (2012). SDO/AIA detection of solar prominence formation within a coronal cavity. *Astrophys. J.* 758, 37. doi: 10.1088/2041-8205/758/2/L37
- Cheng, X., Zhang, J., Saar, S. H., and Ding, M. D. (2012). Differential emission measure analysis of multiple structural components of coronal mass ejections in the inner corona. *Astrophys. J.* 761, 62. doi: 10.1088/0004-637X/761/1/62
- Dere, K. P., Landi, E., Mason, H. E., Monsignori Fossi, B. C., and Young, P. R. (1997). CHIANTI - an atomic database for emission lines. *Astron. Astrophys. Supp.* 125, 149. doi: 10.1051/aas:1997368
- Forland, B. C., Gibson, S. E., Dove, J. B., Rachmeler L. A., and Fan, Y., (2013). Coronal cavity survey: morphological clues to eruptive magnetic topologies. *Sol. Phys.* 288, 603. doi: 10.1007/s11207-013-0361-1
- Fuller, J., Gibson, S. E., de Toma, G., and Fan, Y. (2008). Observing the unobservable? Modeling coronal cavity densities. *Astrophys. J.* 678, 515. doi: 10.1086/533527
- Fuller, J., and Gibson, S. E. (2009). A survey of coronal cavity density profiles. *Astrophys. J.* 700, 1205. doi: 10.1088/0004-637X/700/2/1205
- Gibson, S. E. (2015). "Coronal cavities: observations and implications for the magnetic environment of prominences," in *Solar Prominences, Astrophysics and Space Science Library*, Vol. 415, eds J.-C. Vial and O. Engvold (Springer International Publishing Switzerland), 323.
- Gibson, S. E., Foster, D., Burkepile, J., de Toma, G., and Stanger, A. (2006). The calm before the storm: the link between quiescent cavities and coronal mass ejections. *Astrophys. J.* 641, 590. doi: 10.1086/500446
- Gibson, S. E., Kucera, T. A., Rastawicki, D., Dove, J., and de Toma, G. (2010). Three-dimensional morphology of a coronal prominence cavity. *Astrophys. J.* 724, 1133. doi: 10.1088/0004-637X/724/2/1133
- Gibson, S. E., Kucera, T., White, S. M., Dove, J., Fan, Y., Forland, B. et al. (2016). FORWARD: A toolset for multiwavelength coronal magnetometry. *Front. Astron. Space Sci.* 3:8. doi: 10.3389/fspas.2016.00008
- Habbal, S. R., Druckmueller, M., Morgan, H., Scholl, I., Rusin, V., Daw, A., et al. (2010). Total solar eclipse observations of hot prominence shrouds. *Astrophys. J.* 719, 1362. doi: 10.1088/0004-637X/719/2/1362
- Heizel, P., Schmieder, B., Fárnik, F., Schwartz, P., Labrosse, N., Kotrč, P. et al. (2008). Hinode, TRACE, SOHO, and ground-based observations of a quiescent prominence. *Astrophys. J.* 686, 1383. doi: 10.1086/591018
- Hudson, H. S., Acton, L. W., Harvey, K. A., and McKenzie, D. M. (1999). A stable filament cavity with a hot core. *Astrophys. J.* 513, 83. doi: 10.1086/311892
- Hudson, H. S., and Schwenn, R. (2000). Hot cores in coronal filament cavities. *Adv. Space Res.* 25, 1859. doi: 10.1016/S0273-1177(99)00618-3
- Illing, R. M., and Hundhausen, J. R. (1986). Disruption of a coronal streamer by an eruptive prominence and coronal mass ejection. *J. Geophys. Res.* 91, 10951.
- Jibben, P. R., Reeves, K. K., and Su, Y. (2016). Evidence for a magnetic flux rope in observations of a solar prominence-cavity system. *Front. Astron. Space Sci.* 3:10. doi: 10.3389/fspas.2016.00010
- Lemen, J. R., Title, A. M., Akin, D. J., Boerner, P. F., Chou, C., Drake, J. F., et al. (2012). The Atmospheric Imaging Assembly (AIA) on the Solar Dynamics Observatory (SDO). *Sol. Phys.* 275, 17. doi: 10.1007/s11207-011-9776-8
- Low, B. C. (1994). Magnetohydrodynamic processes in the solar corona: flares, coronal mass ejections, and magnetic helicity. *Phys. Plasmas* 1, 1684. doi: 10.1063/1.870671
- Low, B. C., and Hundhausen, J. R. (1995). Magnetostatic structures of the solar corona. 2: the magnetic topology of quiescent prominences. *Astrophys. J.* 443, 818.
- Maričić, D., Vršnak, B., Stanger, A. L., and Veronig, A. M. (2004). Coronal mass ejection of 15 may 2001: I. evolution of morphological features of the eruption. *Sol. Phys.* 225, 337. doi: 10.1007/s11207-004-3748-1
- Marqué, C. (2004). Radio metric observations of quiescent filament cavities. *Astrophys. J.* 602, 1037. doi: 10.1086/381085
- Marqué, C., Lantos, P., and Delaboudinière, J.-P. (2002). Multi wavelength investigation of the eruption of a sigmoidal quiescent filament. *Astron. Astrophys.* 387, 317. doi: 10.1051/0004-6361:20020309
- McCauley, P. I., Su, Y. N., Schanche, N., Evans, K. E., Su, C., McKillop, S., et al. (2015). Prominence and filament eruptions observed by the solar dynamics observatory: statistical properties, kinematics, and online catalog. *Sol. Phys.* 290, 1703. doi: 10.1007/s11207-015-0699-7
- Pesnell, W. D., Thompson, B. J., and Chamberlin, P. C. (2012). The Solar Dynamics Observatory (SDO). *Sol. Phys.* 275, 3. doi: 10.1007/s11207-011-9841-3
- Reeves, K. K., Gibson, S. E., Kucera, T. A., Hudson, H. S., and Kano, R. (2012). Thermal properties of a solar coronal cavity observed with the X-ray telescope on Hinode. *Astrophys. J.* 746, 146. doi: 10.1088/0004-637X/746/2/146
- Régnier, S., Walsh, R. W., and Alexander, C. E. (2011). A new look at a polar crown cavity as observed by SDO/AIA. Structure and dynamics. *Astron. Astrophys.* 533, L1. doi: 10.1051/0004-6361/201117381
- Schmit, D. J., Gibson, S. E., Tomczyk, S., Reeves, K. K., Sterling, A. C., Brooks, D. H., et al (2009). Large-scale flows in prominence cavities. *Astrophys. J.* 700:L96. doi: 10.1088/0004-637X/700/2/L96
- Su, Y., van Ballegoijen, A., McCauley, P., Ji, H., Reeves, K. K., and DeLuca, E. E. (2015). Magnetic structure and dynamics of the erupting solar polar crown prominence on 2012 march 12. *Astrophys. J.* 807, 144. doi: 10.1088/0004-637X/807/2/144
- Tandberg-Hanssen, E. (1995). *The Nature of Solar Prominences, 2nd Edn.* Dordrecht: Kluwer.

- Tian, H., Tomczyk, S., McIntosh, S. W., Bethge, C., de Toma, G., and Gibson, S. E. (2013). Observations of coronal mass ejections with the coronal multichannel polarimeter. *Sol. Phys.* 288, 637. doi: 10.1007/s11207-013-0317-5
- Tomczyk, S., Card, G. L., Darnell, T., Elmore, D. F., Lull, R., Nelson, P. G. et al (2008). An instrument to measure coronal emission line polarization. *Sol. Phys.* 247, 411. doi: 10.1007/s11207-007-9103-6
- Vaiana, G. S., Davis, J. M., Giacconi, R., Krieger, A. S., Silk, J. K., Timothy, A. F., et al. (1973a). Identification and analysis of structures in the corona from X-ray photography. *Sol. Phys.* 32, 81. doi: 10.1007/BF00152731
- Vaiana, G. S., Krieger, A. S., and Timothy, A. F. (1973b). X-Ray observations of characteristic structures and time variations from the solar corona: preliminary results from SKYLAB. *Astrophys. J.* 185, 47. doi: 10.1086/181318
- Vršnak, B., Maričić, D., Stanger, A. L., and Veronig, A. M. (2004). Coronal mass ejection of 15 may 2001: II. Coupling of the Cme acceleration and the flare energy release. *Sol. Phys.* 225, 355. doi: 10.1007/s11207-004-4995-x
- von Klüber, H. (1961). Photometric investigation of the inner solar corona using an eclipse plate of 1927 June 29. *Monthly Notices R. Astron. Soc.* 123, 61. doi: 10.1093/mnras/123.1.61
- Waldmeier, M. (1941). *Ergebnisse und Probleme der Sonnenforschung*. Leipzig: Becker & Erler kom.-ges.
- Waldmeier, M. (1970). The structure of the monochromatic corona in the surroundings of prominences. *Sol. Phys.* 15, 167.
- Weber, M. A., DeLuca, E. E., Golub, L., and Sette, A. L. (2004). "Temperature diagnostics with multichannel imaging telescopes," in *Multi-Wavelength Investigations of Solar Activity, IAU Symposium*, Vol. 223, eds A. V. Stepanov, E. E. Benevolenskaya, and A. G. Kosovichev (Cambridge, UK: Cambridge University Press), 312–328.
- Wesley, W. H. (1927). *Memoirs of the British Astronomical Association, Vol. 64, Appendix*.
- Williamson, N. K., Fullerton, C. M., and Billings, D. E. (1961). Coronal emission in the vicinity of quiescent prominences. *Astrophys. J.* 133, 973. doi: 10.1086/147102
- Conflict of Interest Statement:** The authors declare that the research was conducted in the absence of any commercial or financial relationships that could be construed as a potential conflict of interest.
- The reviewer CJ and handling Editor declared a past collaboration and the handling Editor states that the process nevertheless met the standards of a fair and objective review.
- Copyright © 2016 Bąk-Stęślička, Gibson and Chmielewska. This is an open-access article distributed under the terms of the Creative Commons Attribution License (CC BY). The use, distribution or reproduction in other forums is permitted, provided the original author(s) or licensor are credited and that the original publication in this journal is cited, in accordance with accepted academic practice. No use, distribution or reproduction is permitted which does not comply with these terms.